Journal of Materials Chemistry C

Accepted Manuscript

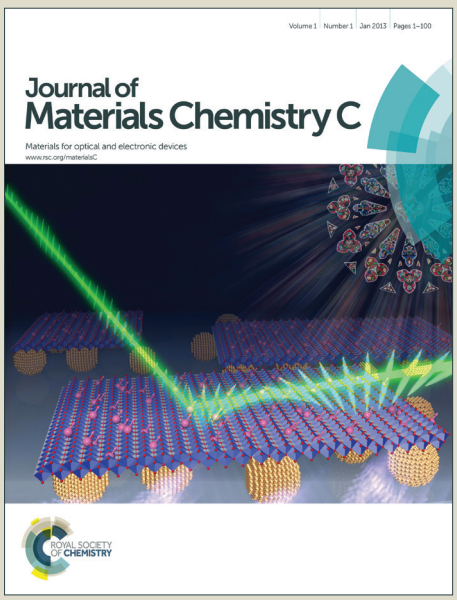

ROYAL SOCIETY OF CHEMISTRY

www.rsc.org/materialsC

Broadband enhanced fluorescence using Zinc-Oxide nanoflower arrays

Tiesheng Wang[1], Jozerd Costan[1], Anthony Centeno[1,2], Mary P. Ryan[1], Fang Xie[1,*]

[1] Department of Materials, Imperial College London, London, United Kingdom, SW7 2AZ.

[2] Malaysia Japan International Institute of Technology, University Technology Malaysia International Campus, 54100 Kuala Lumpur, Malaysia

* Corresponding author: f.xie@imperial.ac.uk

Abstract: ZnO nanostructures were fabricated into flower-like nanoscale arrays by the hydrothermal growth of ZnO nanowires onto a self-assembled monolayer of polystyrene spheres on a glass substrate. Fluorescent molecules conjugated with streptavidin were incubated on glass with 3-(Glycidoxypropyl) trimethoxysilane (GPTS) modified and biotinylated bovine serum albumin (bBSA) attached (GPTS-bBSA), aligned ZnO nanorod arrays and ZnO nanoflower arrays, respectively. An enhancement factor of up to 45 was obtained from ZnO nanoflower arrays, compared to less than 10 for the aligned nanorods. More importantly, using the same substrate, we observed a broadband fluorescence enhancement. The level of enhancement obtained from the nanoflower arrays is comparable with that obtainable from Metal Enhanced Fluorescence. The broadband nature of this process makes it an attractive alternative for fluorescent based device development.

1.Introduction

The use of fluorescent molecules is a common labelling technique in biosensing and bioimaging for the detection of disease biomarkers[1]. Nevertheless there are issues faced by fluorescent molecules in terms of low intensities and photo-stability. In particular the sensitivity of antibody microarrays is critical for the early diagnosis of diseases and improved treatment. Amplification of light from fluorophores by coupling to metal nanostructures, the so called Metal Enhanced Fluorescence (MEF) has been extensively studied [2] and is a promising strategy for improving the detection sensitivity and image contrast enhancement However, its application is limited by high material and fabrication costs and susceptibility to fluorescent quenching under certain conditions [3].

An alternative to MEF is the use of nanostructured Zinc Oxide (ZnO) which is an abundant, non-toxic and inexpensive metal oxide. The strong fluorescence enhancing capability of ZnO nanorods has been demonstrated by a number of researchers. Dorfman *et al.*[4] first reported the use of nano-scaled ZnO as a potential fluorescence detection platform. The ability of aligned and randomly oriented nano-rods, nano-scaled ZnO film to enhance fluorescence has subsequently been reported [5-8], with up to a 20-fold increase in fluorescence intensity having been demonstrated [5, 6].

ZnO forms a rich family of nanostructures including rod-like, belt-like, tube-like, and flower-like (urchin-like) morphologies [8-22]. A wide range of both solution and vacuum deposition methods have been reported for fabricating the nanostructures, such as hydrothermal growth [5, 6, 12, 23], electro-deposition [11], vapour-solid-condensation [20] and chemical vapour deposition [8]. ZnO nanostructures fabricated into flower-like arrays have been shown to have exceptional optical properties[19] and have been fabricated using different approaches, such as modified Kirkendall process, calcination of zinc metal powder, electro-deposition and

hydrothermal growth. Our group recently reported using a monolayer of Polystyrene Spheres (PS) as the scaffold for forming ZnO nano-flowers[19]. This process is advantageous since it enables a versatile control of dimensions and morphologies of the ZnO nanoflowers and control of the core diameter, through modification of the PS diameter. A close-packed PS monolayer can be formed *via* direct assembly or liquid interface-mediated methods [24]. Non-close packed PS arrays can then be prepared from the close-packed PS monolayer using oxygen plasma etching [25, 26].

In this paper we report on fluorescence detection using flower-like ZnO nanoscale arrays and demonstrate large enhancement over the visible spectrum, when compared with aligned nano-rod arrays and glass. diag The fabrication of the nanoflower array is modified from the work reported previously, consisting of the formation of a PS monolayer and hydrothermal growth of ZnO nanorods. Procedures for functionalising the ZnO nanostructures and glass follow the methods reported previously by Hu *et al.* [6] and Xie *et al.* [19]. Samples were modified with 3-(Glycidoxypropyl) trimethoxysilane (GPTS) and attached with biotinylated bovine serum albumin (bBSA) tagging fluorescent molecules. The schematic diagram of the procedure is shown in Figure 1. Fluorophores Alexa Fluor®350, Alexa Fluor®532, Alexa Fluor®647 and Alexa Fluor®750 were used for the fluorescence enhancement measurements.

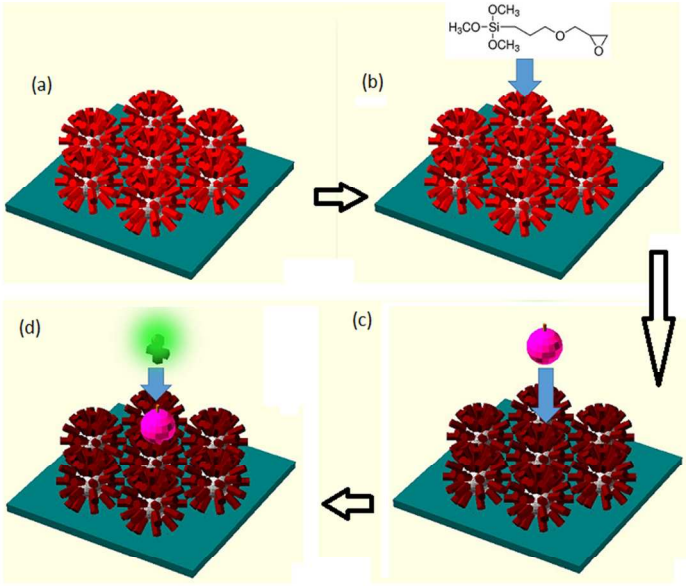

Fig. 1 Schematic Diagram of the sample preparation procedure for fluorescence measurement. (a) ZnO nanoflower arrays formation; (b) GPTS functionalization; (c) biotinlated BSA (bBSA) immobilisation; (d) streptavidin-fluorophore conjugation attachment.

2. Experimental

Materials. Polystyrene spheres (PS) with diameters of 800nm (10 wt. %) were purchased from Bangs Laboratories Inc., USA. The following materials were purchased from Sigma-Aldrich Co. and used as-received: sodium hydroxide (99+%), zinc acetate dihydrate (99+%), 2-aminoethanol (99+%), 2-methoxyethanol (99.8%), zinc nitrate hexahydrate (99+%), hexamethylenetetramine (HMT, 99+%), polyethylenimine branched (PEI), 3-(Glycidoxypropyl)trimethoxysilane (GPTS, 98+%), phosphate buffered saline (PBS) and biotintylated bovine serum albumin (bBSA, 80+%). Ethanol absolute AnalaR

NORMAPUR® (99.8+%), acetone AnalaR NORMAPUR® (99.8+%), 2-Propanol AnalaR NORMAPUR® (99.7+%), potassium chloride (99+%), super premium glass microscope slides were purchased from VWR International, LLC and used as-received. P-Type silicon wafers, boron-doped (with resistivity of 1-5 Ω·cm) were obtained from MMRC Inc. Streptavidin (SA) conjugated dyes, Alexa Fluor® (AF) 350, Alexa Fluor® (AF) 532, Alexa Fluor® (AF) 647 and Alexa Fluor® (AF) 750 were purchased from Invitrogen™. Nanopure water (>18.2M Ω), purified with Milipore Mili-Q gradient system, was used in the experiments.

Formation of non-close-packed Polystyrene Sphere monolayer on a glass substrate. A close-packed polystyrene monolayer was formed using a liquid interface-mediated method. Briefly, commercial PS suspension was diluted with ethanol absolute (1:1) and dropped on to a silicon wafer with one end immersed in water with an inclined angle. The PS was transferred on to alkaline water surface (pH~10) once it was dried. After the transfer was repeated several times, a few drops of surfactant solution were added to condense the PS monolayer. The monolayer was then collected by glass substrates. A non-close-packed PS monolayer was then formed by oxygen plasma etching to obtain a size reduction from 800nm in diameter to 400nm, as described in references [25, 26].

Seed layer formation and hydrothermal growth. The method used for depositing the seed layer for aligned nano-rods was described by Downing et al [10]. Briefly, 0.75M zinc acetate dehydrate and 2-aminoethanol were dissolved in 2-methoxyethanol. Solution film was formed by spin coating at 500rpm for 10s followed by 2000rpm for 30s. Samples were heated on hotplate at 300 ^{o}C for 10min after each coating procedure. Samples were coated 3 times and then annealed at 450 ^{o}C for 60min in a furnace. 0.2 M zinc acetate dehydrate and 2-aminoethanol were dissolved in 2-methoxyethanol for seed layer deposition of nanoflower. The solution film was formed by spin coating at 2000 rpm for 40 s. Samples were annealed at 95^{o}C for 40 min after each coating procedure. Three cycles of coating and annealing were undertaken. Both aligned nanorods and nanoflower were grown in a water bath at approximately 90 ^{o}C for 45 min. The aqueous solution for hydrothermal growth consists of 25mM HMT and zinc nitrate, 200mM potassium chloride and 10 mM PEI. The grown samples were rinsed with purified water and dried naturally.

Functionalization. GPTS treatment of the sample surface was described in the work reported by Hu et al [6,7]. Samples were incubated with diluted GPTS solution (5% v/v in ethanol absolute) for 2h. They were then rinsed with ethanol absolute. The general procedures of bBSA and fluorophore attachment have been described by Xie et al [2]. In summary, samples were incubated with PBS-solution-diluted bBSA solution (100mg/mL, pH~7.2) for 1h. After incubation, samples were rinsed with PBS solution and dried. After bBSA attachment, samples were incubated with PBS-solution-diluted fluorophore (6.25μg/mL) for 2h with light blocker. Samples are finally rinsed with PBS solution and dried.

Characterisation. SEM images were obtained using a LEO Gemini 1525 field emission gun scanning electron microscope (FEG-SEM). The XRD patterns were achieved from X'Pert PRO MPD produced by PANalytical B.V. with 2θ between 30^{o} and 75^{o} and step size of 0.034^{o}. A Copper K^{α} source was used and filtered by Ni. A Nicolet™ iS™10 FT-IR Spectrometer from Thermo Fisher Scientific Inc. was used to obtain infer-red (IR) spectra about GPTS modified glasses, ranging from 1400cm^{-1} to 3400cm^{-1} with bare-glass background subtraction. Low-energy ion scattering (LEIS) using an IONTOF Qtac100 instrument was performed with a 3keV Helium primary ion beam at 5nA, and rastered over an area of 1mm by 1mm. The scattered primary ions were detected at a scattering angle of 145°± 1° over the full azimuth in the energy range of 350eV to 2500eV. Background signals of LEIS patterns were manipulated in approximately the same yield. All fluorescence emission spectra were obtained from unpolarized light using a Fluorolog Tau 3 system from HORIBA Jobin Yvon with 450W Xe lamp excitation. Fluorescence spectra were corrected for the spectral response; scattered excitation light was blocked by long-pass filters.

Table 1. Experimental parameters for fluorescent emission detection.

AF Dye	Excitation Wavelength (nm)	Detection Range (nm)
AF350	385	400-500
AF532	515	540-620
AF647	645	660-750
AF700	700	710-780
AF750	750	765-840

3. Results and discussion

3.1 ZnO nanostructures

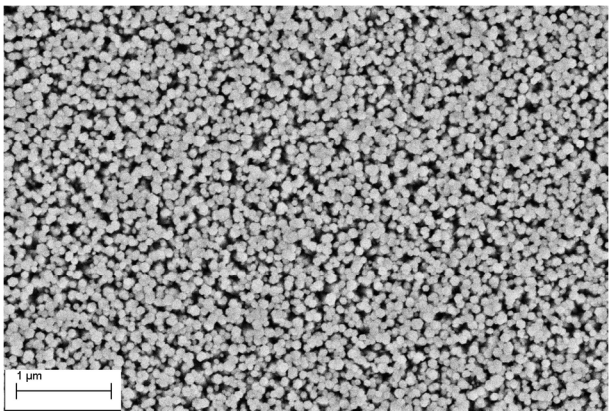

(a)

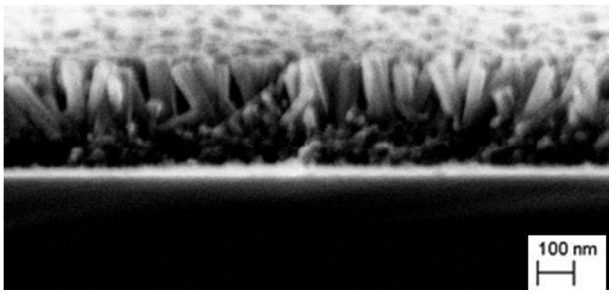

(b)

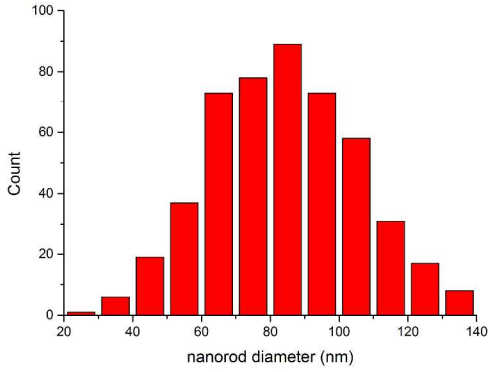

(c)

Figure 1. a) Top view SEM image of aligned nanorods b) side view SEM image of aligned nanorods c) Histogram showing distribution of nanorod diameters (N=490)

Initially ZnO nanorods were grown on a glass substrate to form an aligned array. The reactions involved in the hydrothermal growth of ZnO nanostructures are detailed by Vayssieres [9]. Briefly, HMT decomposes to aldehyde and ammonia. ZnO precipitates owing to the increased pH of the solution. The aligned nano-rods obtained are shown in figure 1. The diameters of the rods with direction (0001) are 83.8 ± 21.5 nm (counted by ImageJ (http://rsbweb.nih.gov/ij/)). The histogram showing the distribution of the diameter is shown in figure 1c. The length of the rods was evaluated to be approximately 170 nm (ImageJ analysis of cross-sectional EM).

Arrays of nanoflowers were then prepared. The PS form a hexagonal close packed (hcp) array, as reported previously [19]. It was observed that the monolayer contains both point and line defects. The morphology of the fabricated nanoflowers is shown in figure 2. The nanoflower array clearly remains in a hexagonal packing pattern (Fig 2a). The diameters of the nanoflowers are 718.5±46.9 nm, shown in the histogram (figure 2c). The diameter of the nano-rods is approximately 65 nm. The diameter of PS after oxygen plasma etching is reduced to approximately 400 nm and the lengths of the nano-rods are approximately 200 nm. Since empty space was created between the individual PS spheres, by oxygen plasma etching, the ZnO nano-rods are able to grow into the gaps, as seen in figure 2b. It can be seen that there is excellent coverage of the polystyrene by the ZnO nanorods (Fig 1a and b).

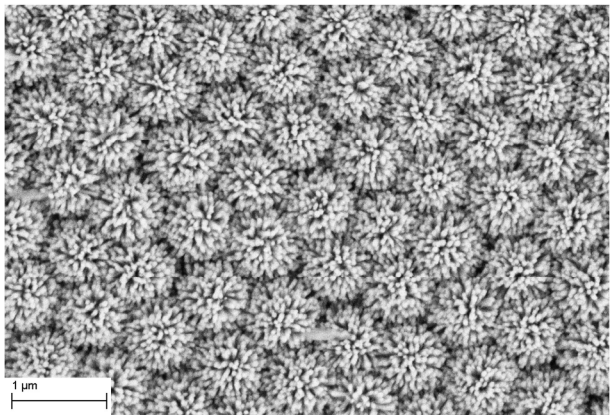

(a)

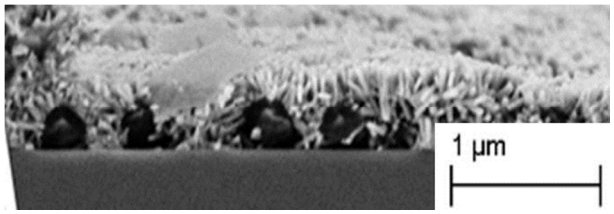

(b)

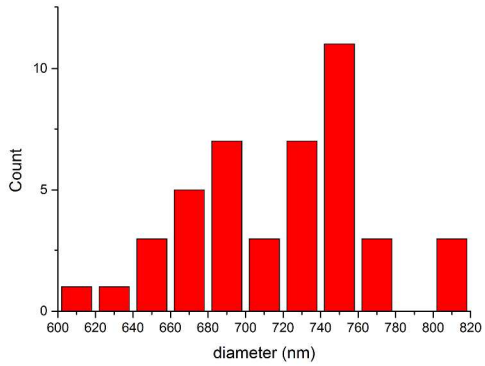

(c)

Figure 2. a) Top view SEM image of nanoflowers b) side view SEM image of nanoflowers c)Histograms showing distribution of nanoflowers diameter (N=44)

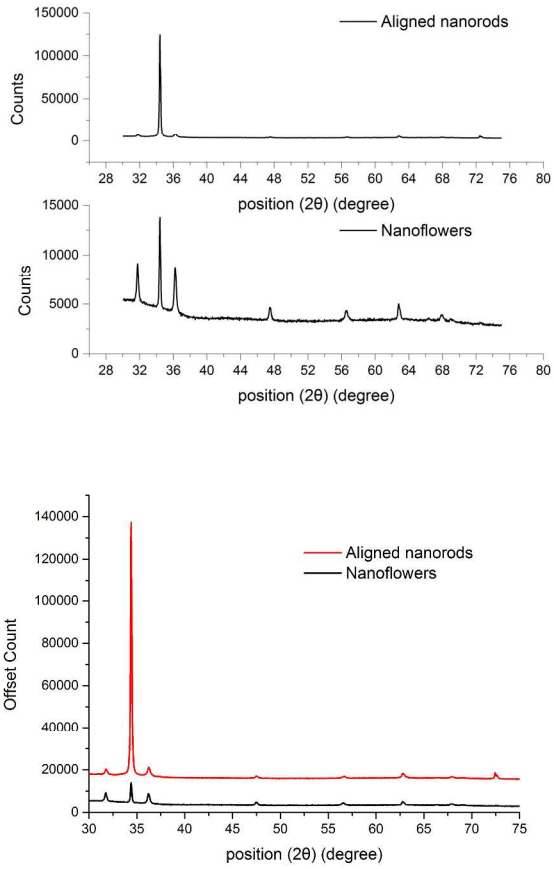

Figure 3. XRD patterns for aligned ZnO nanorods and nanoflowers.

The orientations of the aligned ZnO nanorods and nanoflowers were confirmed using XRD analysis and this is shown in figure 3. For the aligned nano-rods an intense peak at $2\theta \approx 34.5^{o}$ is seen, corresponding to

the (0002) plane which is parallel to the growth direction. This indicates that all the rods are almost well aligned in the same direction. In contrast, XRD pattern for the ZnO nanoflower arrays shows a set of other planes, whilst (0002) plane is still dominant. The results are consistent with XRD data previously reported for aligned and randomly oriented nanorods [6, 10]. An amorphous halo is observed in the region of $2\theta < 40^{o}$ for nanoflowers, most likely due to the presence of polystyrene, although some signal from the glass substrate may also contribute to this.

3.2 Fluorescence detection using nanoflower array and its broadband feature

GPTS and bBSA attachment was verified using glass substrates. Figure 4a shows the IR spectrum of GPTS modified glass, with glass background subtraction. Two significant troughs are shown at 2940 nm and 2838 nm, respectively. These troughs correspond to the presence of methylene on the sample, inferring the attachment of GPTS [6].

Another sample modified by GPTS under the same condition was incubated with diluted bBSA solution. Both the samples were analysed using the IR spectrometer and the samples with bBSA incubation were further analysed by LEIS. LEIS is a non-destructive technique that allows the determination of the outer most atomic layer and in-depth compositional information close to the surface [27]. The results from the two samples are shown in figure 4b. The raw data are normalised to the ion beam current and offset from each other for clarity. It can be seen in figure 4b that three main peaks can be identified in the LEIS data, corresponding to GPTS modified glass. The peaks indicate the presence of C, O, and Si. For the sample incubated with bBSA, the Si peak is no longer observed whilst both the O and C peaks are reduced.

The results show that when the glass is only covered with GPTS the O and Si peaks from the glass are still observed, as the GPTS 'stands' on the surface of the glass and so the glass is still exposed to the primary ion beam. The C, and some of the Si signal, comes from the GPTS. Once the bBSA is introduced the Si signal is supressed, indicating that the glass is covered by the bBSA.

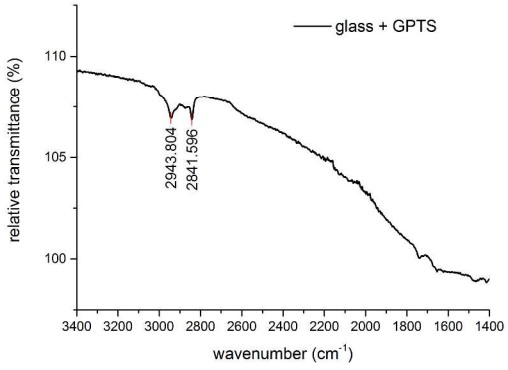

(a)

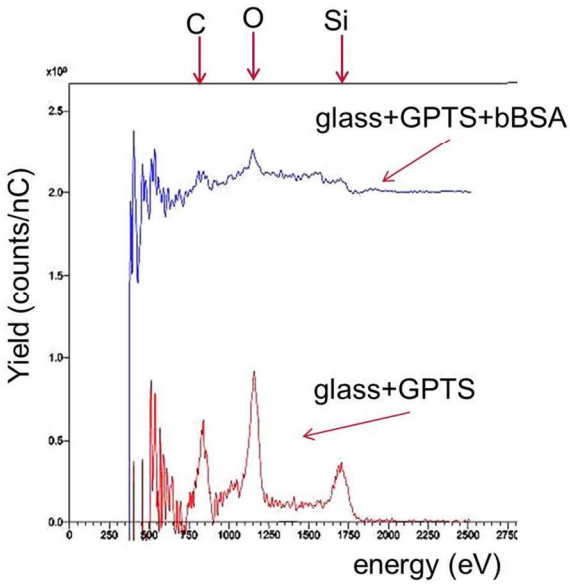

(b)

Figure 4. a)IR spectrum (bare glass background subtracted) of GPTS modified glass b)LEIS patterns (with offset of 2) of GPTS modified glass only (bottom) and GPTS modified glass with bBSA on top (top).

In Figure 5 the fluorescence measurement for the four Alexa Fluor dyes (AF350, AF532, AF647, and AF750) for plain glass, aligned nanorods and nanoflowers are presented. The enhancement factors are summarized in figure 6a and are given by:

$$\text{enhancement factor} = \frac{\text{peak intensity of dye on aligned nanorods or nanoflowers}}{\text{peak intensity of dye on glass}} \quad (1)$$

From figures 5 and 6a it can be seen that there is fluorescent enhancement for all four dyes, which cover the visible part of the electromagnetic spectrum. More importantly, it can be seen that the nanoflower arrays produce a significantly higher enhancement factors, peaking at 45 for AF 647 excited at 645 nm. Initially we assumed that the increase of surface area of the ZnO nanoflower array had a major impact on the enhancement of fluorescence. However, our calculations indicate that for the aligned nanorods the available surface area increases by a factor of 5.70, compared to the flat glass surface, whilst for the nanoflowers it is only slightly larger at 5.77 (The calculations for the increased surface areas due to aligned nanorods and nanoflowers, compared to the flat glass surface are given in the supplementary information). This implies that the increased fluorescent enhancement by the nanoflower arrays cannot be simply accounted by an increased surface area.

The enhancement factor can be normalised by surface area and the results are shown in figure 6b. It can be seen that for AF 350 the normalised enhancement factor is less than 1, for both the aligned nanorods and the nanoflowers, indicating fluorescence quenching. The observation of fluorescence quenching of AF 350 on both ZnO nanoflower arrays and nanorod arrays is expected. This is because the excitation/emission of AF 350 dyes is below the bandgap (375 nm) of ZnO, where ZnO behaves as metal. Consequently, spontaneous emission from fluorophore molecules will be absorbed by ZnO, resulting in no emission from the substrates.

Previous modelling by Börner *et al.* [28] of the evanescent field around ZnO nanorods, with diameters between 300 nm and 1μm, has shown evanescent electric field enhancement close to the surface of the ZnO. Using Finite Difference Time Domain analysis [29] we have investigated the electric field enhancement due to aligned ZnO nanorod arrays excited by a normally incident electric field at wavelengths of 530 nm and 650 nm respectively. The electric field enhancement is found by considering the local electric field at the position and wavelength of excitation, $\mathbf{E}(x_{d,}\lambda_{ex})$ and is given by:

$$\chi = \frac{|\,\mathrm{E}(x_d, \lambda_{ex})\,|^2}{|\,\mathrm{E_i}\,|^2} \qquad (2)$$

where E_i is the incident field magnitude.

The model consisted of nanorods with a diameter of 70 nm and 170 nm in height. The centre to centre spacing of the nanowires was varied. Figures 7a and 7b shows the electric field enhancement for 150 nm separation for excitation at 530 nm and 650 nm respectively. Comparing the two figures it can be seen that the electric field enhancement between the nanowires is higher for the excitation at 650 nm. This enhanced electric field will lead directly to increased excitation of the fluorophore molecules [19] and the increased fluorescent enhancement factors obtained for AF 532 and AF 647 can be qualitatively explained by the enhancement of the near (evanescent) electric field. Another pathway leading to fluorescence enhancement may originate from waveguiding nature of metal oxides. It has been demonstrated that ZnO has shown exceptional UV and visible light-guiding.[30-31] Fluorescence will be enhanced on ZnO substrate due the the direct fluorescence from the fluorophores as well as guided fluorescence from ZnO nanowires, owing to the capability of metal oxides by guiding visible light in and out of fluorophores as well as along the nanowires.[31] The wave guiding property and their ability to enhance the evanescent field may explain the remarkable fluorescence enhancement on ZnO arrays, but it did not explain why ZnO nanoflower array has significantly higher fluorescence enhancement factors. In our previous study,[19] we had a complete investigation of the optical properties of ZnO nanoflower arrays as well as nanorod arrays. It was observed that the diffuse reflection is dominant. This indicates a strong degree of randomness of nanorod alignment in the nanoflower array [19]. Therefore, it is highly likely that scattering property of nanoflower arrays serve as efficient evanescent waveguides enhacing the absorption and emission processes of fluorophores, which in turn enables the nanoflower array significantly higher fluorescence enhancement.

ZnO nanoflower arrays fabrication is scalable and inexpensive. In this work we have not attempted to optimise the nanorod or array dimensions for maximum fluorescent enhancement. Nevertheless we have obtained fluorescent enhancement of the AF532, AF 647 and AF750 flurophores between 25 and 45. This is comparable with that obtained using metal enhanced fluorescence [2]. Much of this enhancement is due to the increased surface area offered by the nanorods, compared to a flat surface. Nevertheless, even after normalizing for surface area it is seen that for the nanoflowers there is still around an order of magnitude enhancement for AF 647. One of the advantages of using ZnO nanoflower arrays for fluorescent enhancement is that the same array could potentially be applied for over a broad band of wavelengths. Consequently, a number of different dyes could be detected in sensing platform. In contrast, metal enhanced fluorescence enhancement requires high degree of overlapping of plasmonic peak of metal to excitation/emission of dyes. As a result, it is a narrow band technique without capacity for multiplexing.

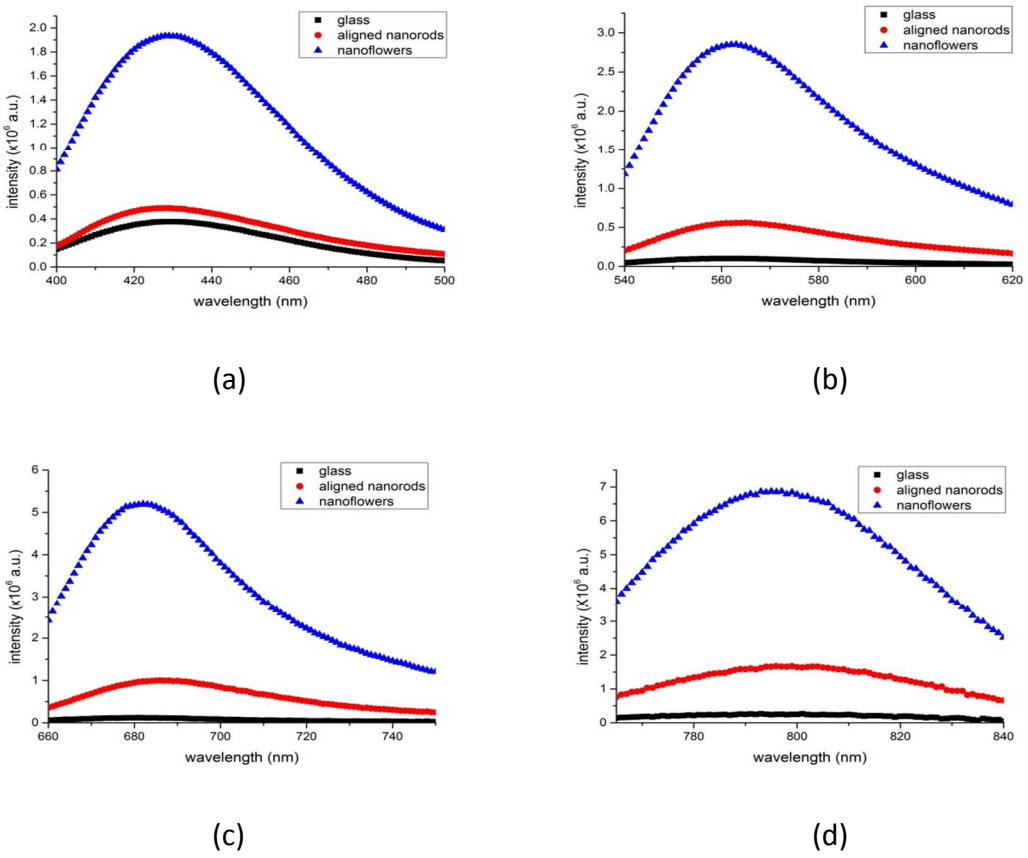

Figure 5. Fluorescence spectra of (a) Alexa Fluor 350 (b) Alexa Fluor 532 (c) Alexa Fluor 647 (d) Alexa Fluor 750 for a glass control (black squares), aligned nanorods(red circles) and nanoflowers (blue triangles).

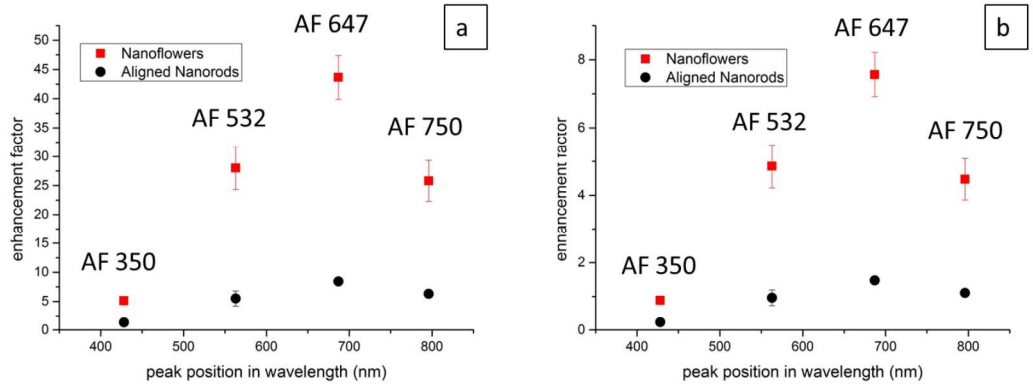

Figure 6. Enhancement factors of aligned nanorods and nanoflowers using different fluorophores: a) without any normalisation; b) normalised by surface area. All error bars are included in the graph, though some of them are too small to show.

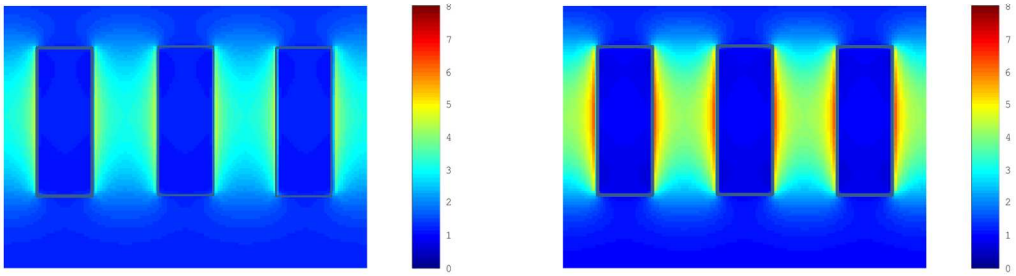

Figure 7. Electric field enhancement due to aligned ZnO nanorods of diameter 70 nm and height 170 nm for an electric field normally incident and polarized parallel to the top surface of the nanowires. Figure 7a and 7b show the enhancement at for centre to centre separations of 150 nm and wavelengths of (a) 530 nm and (b) 650 nm, respectively.

Conclusion

In summary, a modified fabrication process for the controllable production of tunable nanoflower like arrays is reported. The fluorescent enhancement compared to dyes on a glass substrate and aligned nanorods has been investigated. The results show that the nanoflower arrays significantly enhance the fluorescence of various dyes across the entire visual part of the electromagnetic spectrum. The enhancement factor obtained is up to 45 for AF 647 excited at 645 nm. The broadband fluorescence enhancement nature makes them an attractive candidate for multiplexed assay detection. This level of enhancement factor is comparable with that obtained using metal enhanced fluorescence, with the significant advantage of multiplex detection.

References

1. J.R.Lakowicz, in *Probe Design and Chemical Sensing*. ed. J.R. Lakowicz, Plenum Press, New York, 1994, Probe Design in Chemical Sensing, Vol.4.
2. F. Xie, J Pang, A. Centeno, M.P. Ryan, D.J. Riley and N.M. Alford, Nano Research, 2013, **6** , 496-510.
3. S.T. Kochuveedu and D.H. Kim, Nanoscale, 2014, **6**, 4966-84.
4. A. Dorfman, N. Kumar and J. Hahm, Advanced Materials, 2006, **18**, 2685-2690.
5. Y-S. Liu, Y. Fu, B. Ramachandram, R. Joseph, J.R. Lakowicz, and X Xiao-Liange, Chinese Physics B, 2012, **21**, 037803.
6. W. Hu, Y. Liu, Z. Zhu, H.Yang and C. Ming, ACS Applied Materials & Interfaces, 2010, **2**, 1569-1572.
7. W. Hu, Y. Liu, H.Yang, X.Zhou and C.M. Li, ZnO Biosensors and Bioelectronics 2011, **26**, 3683-3687.
8. V. Adalsteinsson, O. Parajuli, S. Kepics, A. Gupta, W.B. Reeves, and J. Hahm, Analytical Chemistry, 2008, **80**, 6594-6601.
9. L. Vayssieres, Advanced Materials, 2003, **15**, 464-466.
10. J.M. Downing, M.P. Ryan and M.A. McLachlan, Thin Solid Films, 2013, **539**, 18-22.
11. R. Könenkamp, K. Boedecker, M.C. Lux-Steiner, M. Poschenrieder, F. Zenia, C. Levy-Clement, and S. Wagner, Applied Physics Letters, 2000, **77**, 2575-2577.
12. A.I. Danciu, V. Musat, T. Busani, J.V. Pinto, R. Barros, A.M. Rego, A.M. Ferraria, P.A. Carvalho, R. Martins and E. Fortunato, J Nanosci Nanotechnol, 2013, **13**, 6701-10.

13. D.F. Zhang, L.D. Sun, J.L. Yin, C.H. Yan and R.M. Wang, J Phys Chem B, 2005, **109**, 8786-90.
14. W.P. Zheng, R.D. Zu, and L.W. Zhong, Science, 2001, **291**, p. 2.
15. Y. Sun, N.G. Ndifor-Angwafor, D.J. Riley and M.N.R. Ashfold, Chemical Physics Letters, 2006, **431**, 352-357.
16. K.W. Chae, Q. Zhang, J.S. Kim, Y.H. Jeong, G. Cao, Beilstein Journal Nanotechnology, 2010, **1**, p. 6.
17. G.W. She, X.H. Zhang, W.S. Shi, X. Fan and J.C. Chang, Electrochemistry Communications, 2007, **9**, 2784-2788.
18. G.W. She, X.H. Zhang, W.S. Shi, X. Fan, J.C. Chang, C.S. Lee, S.T. Lee, C.H. Liu, Applied Physics Letters, 2008, **92**, 05311.
19. F. Xie, A. Centeno, B. Zou, M.P. Ryan, D.J. Riley and N.M. Alford, Journal of Colloid and Interface Science, 2013, **395**, 85-90.
20. J.Shi, H. Hong, Y. Ding, Y. Yang, W. Cai, and X. Wang, Journal of Materials Chemistry, 2011, **21**, 9000-9008.
21. Y.H. Ko and J.S. Yu, J.S.Optics Express, **2011**, 19(27), p. 25935-25943.
22. R.C. Pawar, J.S. Shaikh, S.S. Suryavanshi and P.S. Putil, et al., Current Applied Physics, 2012, **12**, 778-783.
23. W. Wu, G. Hu, S. Cui, Y. Zhou and H. Wu, Crystal Growth & Design, 2008, **8**, 4014-4020.
24. N. Vogel, C.K. Weiss and K. Landfester, Soft Matter, 2012, **8**, 4044-4061.
25. A.Plettl, F.Enderle, M.Saitner, A. Manzke, C. Pfahler, S. Wiedemann and P. Ziemann, Advanced Functional Materials, 2009, **19**, 3279–3284.
26. N. Vogel, S. Goerres, K. Landfester and C.K. Weiss, Macromolecular Chemistry and Physics, 2011, **212**, 1719-1734.
27. H.H.Brongersma, Low-Energy Ion Scattering, in Characterisation of Materials, **2002**, John Wiley and Sons, Inc.
28. S. Börner, C.E. Rüter, T. Voss, D. Kip and W. Schade, Physica Status Solidi (a), 2007, **204**, 3487-3495.
29. A.F. Oskooi, D. Roundy, M. Ibanescu, P. Bermel, J.D. Joannopoulos and S.G. Johnson, Comput. Phys. Commun., 2010, **181**, 687-702.
30. M. Law, D.J. Sirbuly, J.C Johnson, J Goldburger, R.J. Saykally, P.Yang, Science, 2004, 305, 1269 - 1273
31. D.J. Sirbuly, M. Law, P. Pauzauskie H. Yan, A.V. Maslov, K. Knutsen, C.Z. Ning, R.J. Saykally, P.Yang, Proc. Natl. Acad. Sci. 2005, 102, 7800 - 7805

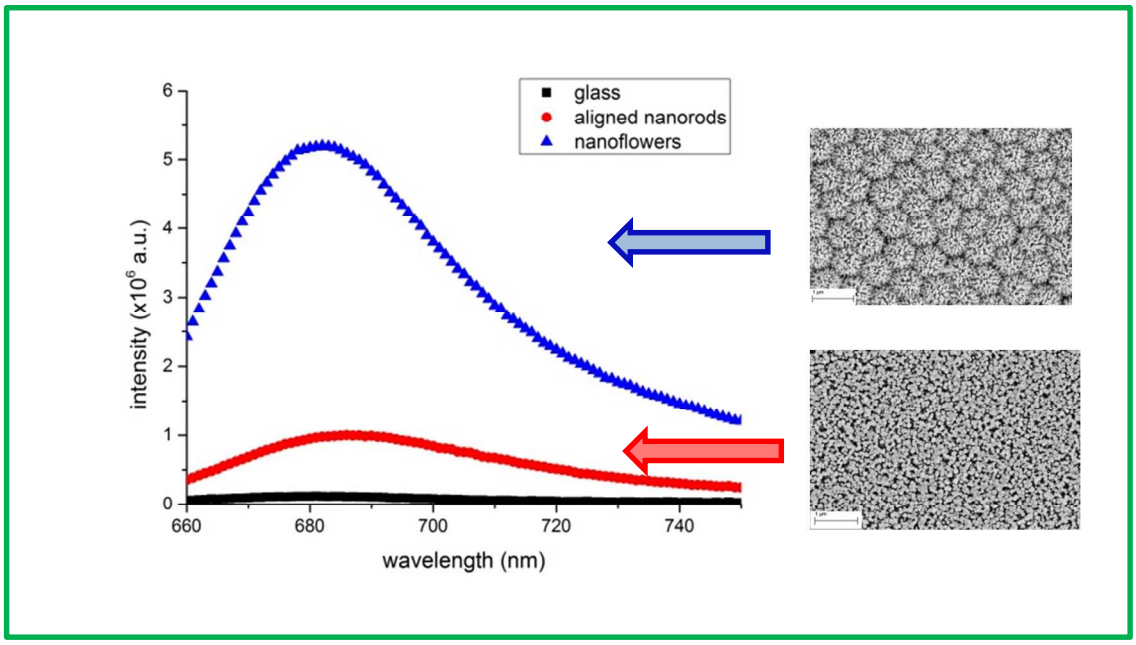

ZnO nanoflower arrays have significantly higher fluorescence enhancement than ZnO nanorod arrays, with broadband enhancement capability.